Cascade Damages and Their Kinetic Behavior in Ceramics Irradiated with Fission- and Fusion-Neutrons

Cascade Damages and Their Kinetic Behavior in Ceramics Irradiated with Fission- and Fusion-Neutrons

Chiken Kinoshita*, Kiyomichi Nakai*, Ken-ichi Fukumoto*,
Masanori Kutsuwada* and Kazuhiro Nogita*
(Received January 28, 1991)

Synopsis

The cascade damage and its kinetic behavior in various kinds of ceramics irradiated with fission- and fusion-neutrons have been examined through transmission electron microscopy. Fission- and fusion-neutrons introduce relatively dilute concentration of point defects around primary knock-on atoms through the displacement cascade process in low-Z ceramics. Higher concentration of point defects, which induces the contrast corresponding to the cascade damage though TEM, is induced only in covalent crystals consisting of relatively high-Z elements. The nucleation and growth process of interstitialloops is strongly affected by the crystal structure and structural vacancy.

I. Introduction

There has been increased interest in recent years in studying radiation effects in ceramics, because of their potential use for a variety of nuclear applications. These ceramic materials will be required to maintain electrical and structural integrity under fast neutron irradiation in the fluence range of 10^{23} - 10^{28} n/m^2 at various temperatures.[1] However, little definitive experimental work has been done on the cascade damages produced by fast neutrons and their kinetic behavior, which are the most important information for understanding the radiation damage in materials.

Ceramic materials most frequently are ionic or covalent crystals and have their own particular characteristics, such as polyatomicity, the necessity to preserve electrical neutrality, the reciprocity between defect structure and stoichiometry, the existence of a charge state on point defects, and the radiation-induced bias. These characteristics together with high impurity contents make radiation phenomena in ceramics more complicate than metals. On the

* Department of Nuclear Engineering, Faculty of Engineering, Kyushu University, Fukuoka 812

other hand, it may be also true that some of these characteristics are effective to suppress the radiation damage and are important for designing radiation-resistant materials.[2)]

Stimulated by these great interest and importance, systematic experiments were designed for finding out effects of fission- and fusion-neutron irradiation on ceramics. The objective is to obtain the knowledge of the cascade damages and their kinetic behavior in various kinds of ceramics through transmission electron microscopy (TEM). The focus of scientific interest is the effects of the crystal structure, the atomic bonding, the structural vacancy, the mass ratio of constituent elements and the impurity on the structure of cascade damages and their stability and kinetic behavior.

II.Experimental

This is one of systematic experiments designed by Japanese research groups for finding out 14 MeV neutron irradiation effects of ceramics, and is based on the results of the first run conducted by Kiritani.[3)] Because of little definitive works on cascade structures in ceramics, it is desired to prepare various kinds of ceramics, as much as possible. The following materials including ceramics and semiconductors were kindly prepared by researchers at universities and institutes or supplied by companies;

MgO(S), MgO(Li-doped)(S), MgO(Ni-doped)(S), MgO(Co-doped)(S), MgO(Fe-doped)(S), MgO(Cr-doped)(S), MgO(P,A), MgO(P,B), Al_2O_3(S), Al_2O_3(P,A), Al_2O_3(P,B), Al_2O_3(P,C), Al_2O_3(P,D), $MgAl_2O_4$(S), $MgO \cdot 1.2Al_2O_3$(S), $MgO \cdot 3.0Al_2O_3$(S), Mg_2SiO_4(S), Y_2O_3-92%ZrO_2(S), Y_2O_3-88%ZrO_2(S), Y_2O_3-85.5%ZrO_2(S), Y_2O_3(S), ZrO_2(P,A), ZrO_2(P,B), ZrO_2(P,C), TiO_2(S), SiO_2(S), NiO(S), CoO(S), Cr_2O_3(S), $2MgO \cdot 2Al_2O_3 \cdot 5SiO_2$(P), Al_2O_3-SiO_2(P), Al_2O_3-30%TiO_2(P), $Y_2Al_5O_{12}$(S), $Gd_3Ga_3O_{12}$(S), $SrTiO_3$(S), $Bi_{12}GeO_{20}$(S), SiC(S), SiC(P,A), SiC(P,B), SiC(P,C), SiC(P,D), TiC_{1-x}(P,A), TiC_{1-x}(P,B), TiC-14%Mo(S), TiC-25%Mo(S), Cr_3C_2(P), WC(P), B_4C(P), Graphite(P), C-10%B_4C(P), C-20%B_4C(P), C-30%B_4C(P), C-20%SiC(P), Sialon(Z=1)(P,A), Sialon(Z=1)(P,B), Sialon(Z=3)(P), Si_3N_4(P,A), Si_3N_4(P,B), Si_3N_4(P,C), Si_3N_4(P,D), AlN(P), TiN(P), TiB_2(P), Si(S,A), Si(S,B), Si(S,C), Al_2O_3/Nb(P).

Here, S and P in the parentheses stand for single crystals and poly- or sintered crystals, respectively. Furthermore, A, B, C or D represents the source of crystals.[4)]

As-received materials were cut into thin wafers approximately 500 μm in thickness. Those wafers were cut out into 3 mm discs with an ultrasonic drill. The resultant discs were mechanically thinned with SiC papers and 3 μm Al_2O_3 powders to final thickness of

100~200 μm. Those discs, 3 mm in diameter, were then chemically polished (MgO) or electro-polished (TiC_{1-x}) to electron transparency. Ion beam milling was used to prepare TEM specimens, whenever chemical- or electro-polishing could not be employed. In order to reduce the ion milling time, the dimple-like depression, which is referred to as 'dimpling', was produced with a dimpler (G-Model D 400) and 1~3 μm diamond compound, and discs were locally pre-thinned to 10~50 μm thickness surrounded by each periphery of about 200 μm thick materials.

About 300 specimens for electron microscopy and some other types of specimens for optical measurements, which consist of 67 kinds of single crystals or poly-crystals, were irradiated in air at 300 K with D-T neutrons produced by RTNS-II. Some of specimens were irradiated in a vacuum at 473 K and 723 K in a run conducted by Yoshiie and Kawanishi.[5] Some TEM specimens of SiC, TiC, $MgAl_2O_4$ and Al_2O_3, on the other hand, were sealed into evaluated silica tubes, and irradiated with fission neutrons at 673, 773 and 873 K in Joyo (Fast Breeder Testing Reactor in Japan) up to 1×10^{24}, 1×10^{25} or 9×10^{25} n/m^2.

In order to avoid the effect of ion beam milling, irradiated specimens were sometimes sputtered with 2~3 keV Ar^+ ions or crushed into powder in an alumina mortar. The powder was suspended in n-propyl alcohol and the suspension with the powder was dropped on TEM microgrids with a syringe. After microgrids were naturally dried in a vacuum, they were subjected to TEM observations at room temperature. Irradiated specimens were observed with electron microscopes JEM-200CX in Lawrence Livermore National Laboratory and Oarai Branch for JMTR Utilization of Tohoku University, or with a JEM-2000EX in the RI Center at Kyushu University. In the case of non-irradiated specimens, a JEM-200BS in the HVEM Lab. at Kyushu University was used. In the TEM observation, the microstructural evolution induced by irradiation was not influenced by the pulverization of specimens. The use of powder specimens was found to be convenient for TEM observation of neutron irradiated ceramics and to have the advantage in dealing with small amount of radioactive materials.

III.Results and discussion

When fast neutrons are irradiated to crystals, they tranfer their kinetic energy to primary knock-on atoms(PKA). One of characteristics of neutron irradiation is cascade damages produced by high-energy PKA. The structure of cascades and their accumulation process together with the effects of low-energy PKA or electron excitation on cascades

produced by high-energy PKA are important.

Weak-beam electron microscopy has been extensively applied to the observation of strain contrast in specimens irradiated with 14 MeV neutrons. Results on irradiated specimens are divided in three groups. (1) White contrast is observed in TiN, MgO, WC, $MgAl_2O_4$ and Y_2O_3-88%ZrO_2 just after the irradiation at 300 K and it is also observed in $TiC_{0.85}$ after the irradiation at 473 and 723 K, as shown in fig. 1. The contrast in Y_2O_3-88%ZrO_2, WC and $TiC_{0.85}$ may be due to the first finding of cascade damages in ceramics. However, more careful works are required for getting conclusive remarks. The contrast appeared in TiN, MgO and $MgAl_2O_4$ is due to oxidation or defect clusters induced during 6 keV Ar^+ sputtering. (2) No strain contrast is observed, but the contrast appears during illumination of 200 keV electrons at 300 K in $TiC_{0.85}$, AlN, Cr_2O_3 and SiO_2 irradiated with 14 MeV neutrons at 300 K. Typical examples of sequences are shown in fig. 2 and fig. 3 for SiO_2 and Cr_2O_3, respectively. The illumination of lower energy electrons induces more precipitaiton of amorphous phase in SiO_2 and AlN through the radiolysis, and relaxes cascades in $TiC_{0.85}$ and SiC to make observable configurations. In the case of Cr_2O_3, interstitials induced by knock-on or electronic excitation under the electron illumination aggregate as interstitial clusters. (3) No strain contrast has been detected even during electron illumination for 2 ks at 300 K in Al_2O_3-30%TiO_2. Interstitial loops as large as 10 nm in diameter were introduced in $MgAl_2O_4$ through the nucleation and growth process during irradiation with 14 MeV neutrons of 5×10^{22} n/m^2 at 723 K, and are shown in fig. 4. Dual-beam irradiation with 30 keV Xe^+ ions and fast electrons have been performed by Abe et al.[6] for predicting which ceramics show up the contrast corresponding to cascade damages in TEM. According to their results, contrasts corresponding to individual displacement cascades are induced in TEM only for covalent crystals which consist of relatively high-Z elements. The results on 14 MeV neutron irradiation don't contradict with the prediction by Abe.[6]

The nucleation and growth of defect clusters in various kinds of ceramics under fast electron irradiation has been found to be affected by the crystal structure, the structure vacancy and the bond type, and it has been classified into (1) the MgO type, (2) the TiC type, (3) the spinel type and (4) the graphite type.[2] Analogous studies have been performed through the microstructural evolution of defect clusters in various ceramic materials irradiated with fission neutrons. Figure 5 (A), (B), (C) and (D) are typical examples of weak-beam dark-field images, showing defect clusters in SiC, $TiC_{0.85}$, $MgAl_2O_4$ and Al_2O_3 irradiated in Joyo, respectively. Small defect

clusters are observed in $TiC_{0.85}$, $MgAl_2O_4$ and Al_2O_3, but tiny faint contrasts are seen in the micrograph of SiC. Among these materials, $TiC_{0.85}$ and $MgAl_2O_4$, which belong respectively to the TiC type and the spinel type, were extensively studied, because of their low-swelling character based on characteristics of those types.

Figure 6 shows defect clusters developping into interstitial loops and tangled dislocations with increasing the irradiation temperature and/or the fluence. The size distribution of loops in $TiC_{0.85}$ irradiated with fission neutron fluence of 1×10^{24} n/m^2 at 673 K is shown in fig. 7. The concentration of interstitials contained in loops is estimated to be 0.06 % on the assumption that 1×10^{25} n/m^2 corresponds to 1 dpa, and predict effective recombination of displaced atoms with structural vacancies.

Figure 8 shows small dot contrasts and large dislocation loops in $MgAl_2O_4$ irradiated at 673, 773 and 873 K with neutron fluence of 1×10^{24}, 1×10^{25} and 9×10^{25} n/m^2. Small dot contrasts are corresponding to small dislocation loops. Large dislocation loops were detected to be interstitial dislocation loops with Burgers vectors b=1/4 <110> on {110} planes through the g-b analysis. However, no voids were observed. In TEM observations, $MgAl_2O_4$ specimens irradiated with neutrons were again illuminated with 200 keV electrons. Illumination with 200 keV electrons eliminates dislocation loops shown in fig. 8(A) for $MgAl_2O_4$ irradiated with fission neutrons at 673 K, as shown in fig. 9, but it scarcely alters the morphology of 1/4 <110>/{110} loops in fig. 8(E). Hobbs and Clinard[7] reported that there were two types of dislocation loops in the neutron irradiated $MgAl_2O_4$; these were stable interstitial dislocation loops with b=1/4 <110> and unstable ones with b=1/6 <111>. In a previous study, Satoh et al.[8] reported that irradiation with 7 keV Ar^+ ions induced tiny clusters in $MgAl_2O_4$, which were mostly 1/6 <111> interstitial loops, and that these loops were not stable under irradiation with 1000 keV electrons. It is considered, therefore, that unstable dislocation loops in fig. 8(A) and fig. 9 are of interstitial type with b=1/6 <111> and that most of them disappear during neutron irradiation at higher temperatures.

Figure 10 shows the size distribution of dislocation loops in $MgAl_2O_4$ irradiated at 673 K and 773 K with neutron fluences of 1×10^{25} n/m^2 and 9×10^{25} n/m^2. The size and the density of dislocation loops increases and decreases respectively with increasing the irradiation temperature and the neutron fluence. Since fission neutron fluence of 1×10^{25} n/m^2 approximately corresponds to 1 dpa, the corresponding fraction of displacements retained in the form of dislocation loops is 6.5×10^{-3} to 1.5×10^{-2} % under those irradiation

conditions. It is well known that $MgAl_2O_4$ is low-swelling material. $MgAl_2O_4$ contains high concentration of structural vacancies, so that defect clusters are hardly formed because of the recombination of excess structural vacancies with the interstitials induced by irradiation. Furthermore, interstitial dislocation loops have less chance to nucleate or to grow in $MgAl_2O_4$, because of large and stoichiometric nuclei of 1/4 <110> loops and/or instability of 1/6 <111> loops. The results of this study can be correspondingly considered to hold the same view of these characteristics of $MgAl_2O_4$.

IV. Summary

It is well known that the lower-Z ceramic materials slow down fast neutrons more effectively. Therefore, a portion of high-energy PKA becomes large and the flux of low-energy neutrons becomes more dominant rather than that of 14 MeV neutrons for those ceramic materials. Furthermore, the fraction of the PKA energy dissipated for electronic excitation becomes more dominant. From those viewpoints, the difference between characteristics of 14 MeV neutrons and those of fission neutrons are based on electronic excitation as well as transmutation rather than the displacement process in those materials. Even high-energy PKA produce relatively dilute concentration of point defects within cascades and induce relatively homogeneous distribution of point defects in low-Z ceramics. However, in higher-Z covalent crystals, amorphous-like phase or defect clusters are induced. Also, in ionic crystals, high-energy PKA provide nuclei of interstitial clusters, and the nucleation process of those defect clusters is affected by the crystal structure, the structural vacancy and low-energy PKA. The polyatomicity as well as the structural vacancies are effective to suppress the nucleation and the growth of defect wclusters.

References

(1) G.R. Hopkins and R.J. Price, Nucl. Eng. Des./Fusion, 2(1985),111
(2) C. Kinoshita and K. Nakai, Jpn. J. Appl. Phys. Series 2 Lattice Defects in Ceramics, 1989, p.105.
(3) M. Kiritani, J. Nucl. Mater., 133-134 (1985), 85.
(4) C. Kinoshita, Annual Research Report of Japanese Contributions for Japan-US Collaboration on RTNS-II Utilization, 1990, p.155.
(5) M. Kiritani, ibid, 1988, p.1.
(6) H. Abe, C. Kinoshita and K. Nakai, J. Nucl. Mater., 179-181(1991), in press.
(7) L.W. Hobbs and F.W. Clinard Jr., J. Physique, 41(1980), C6-232.
(8) Y. Satoh, C. Kinoshita and K. Nakai, J. Nucl. Mater., 179-181 (1991), in press.

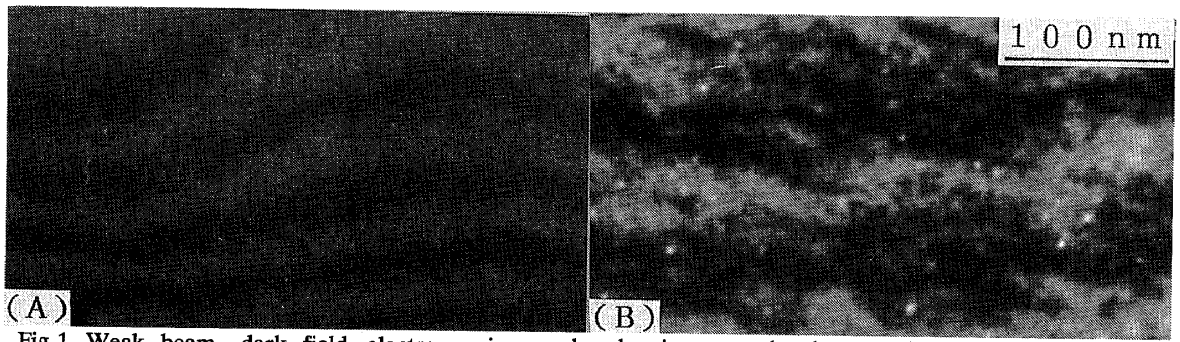

Fig.1 Weak-beam dark-field electron micrographs showing cascade damages in $TiC_{0.85}$ irradiated with 14 MeV neutrons of 5×10^{22} n/m^2 at (A) 473 and (B) 723 K. The specimens were electro-polished before the irradiation.

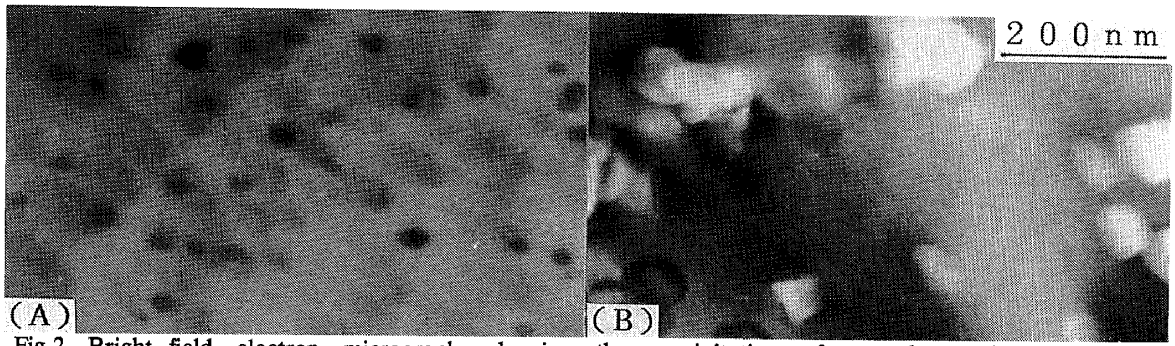

Fig.2 Bright-field electron micrographs showing the precipitation of amorphous phase in SiO_2 under illumination at 300 K with 200 keV electron fluences of (A) 1×10^{24} and (B) 4×10^{24} e/m^2. The electron illumination was performed after irradiation with 14 MeV neutrons of 3.2×10^{21} n/m^2 at 300 K. The specimen was ion-thinned with 2-3 keV Ar^+ after the irradiation.

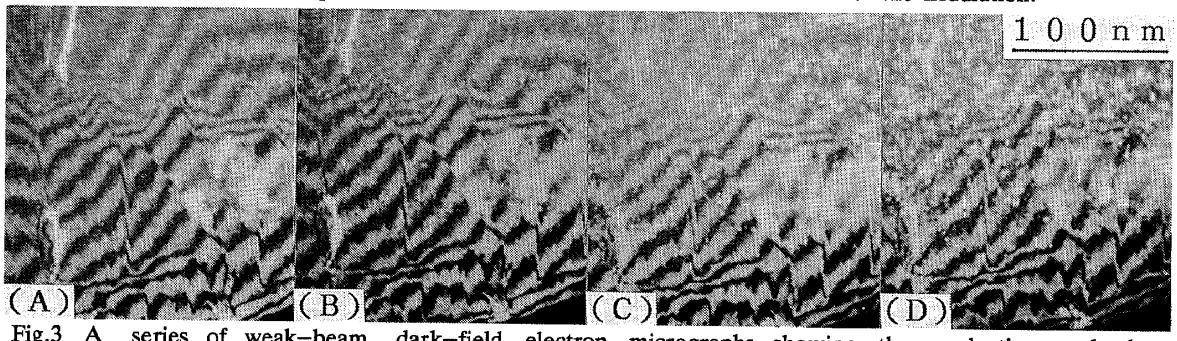

Fig.3 A series of weak-beam dark-field electron micrographs showing the nucleation and the growth of dislocation loops in Cr_2O_3 during 200 keV electron illumination of (A) 1×10^{22}, (B) 3×10^{24}, (C) 1×10^{25} and (D) 3×10^{25} e/m^2 at 300 K. The electron illumination was performed after irradiation with 14 MeV neutrons of 6.6×10^{21} n/m^2 at 300 K. The specimen was crushed into powder after the irradiation.

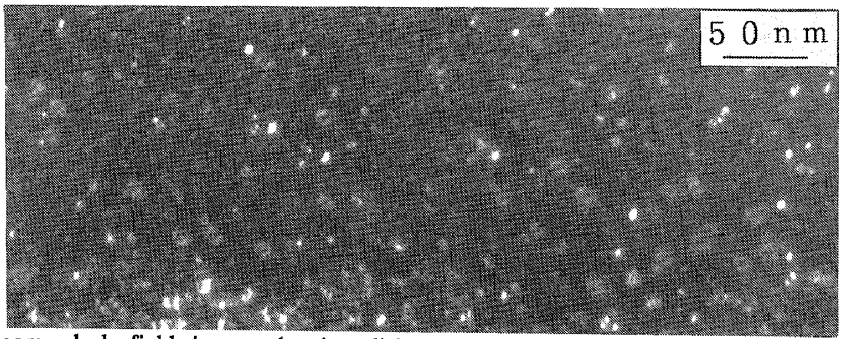

Fig.4 Weak-beam dark-field image showing dislocation loops in $MgAl_2O_4$ irradiated with 14 MeV neutron fluence of 5×10^{22} n/m^2 at 723 K. The Specimen was ion-thinned with 2-3 keV Ar^+ before the irradiation.

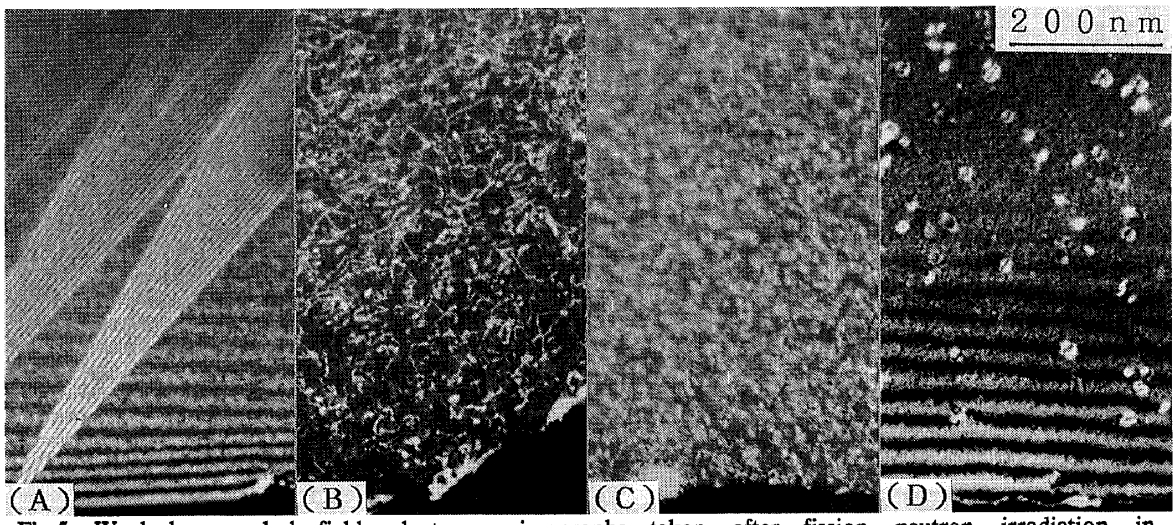

Fig.5 Weak-beam dark-field electron micrographs taken after fission neutron irradiation in Joyo for (A) SiC, (B) $TiC_{0.85}$, (C) Al_2O_3 and (D) $MgAl_2O_4$. Irradiation conditions are as follows ; (A) 1×10^{25} n/m^2 at 773 K, (B) 9×10^{25} n/m^2 at 673 K, (C) 1×10^{25} n/m^2 at 673 K and (D) 1×10^{25} n/m^2 at 673 K. All specimens were crushed into powder after the irradiation.

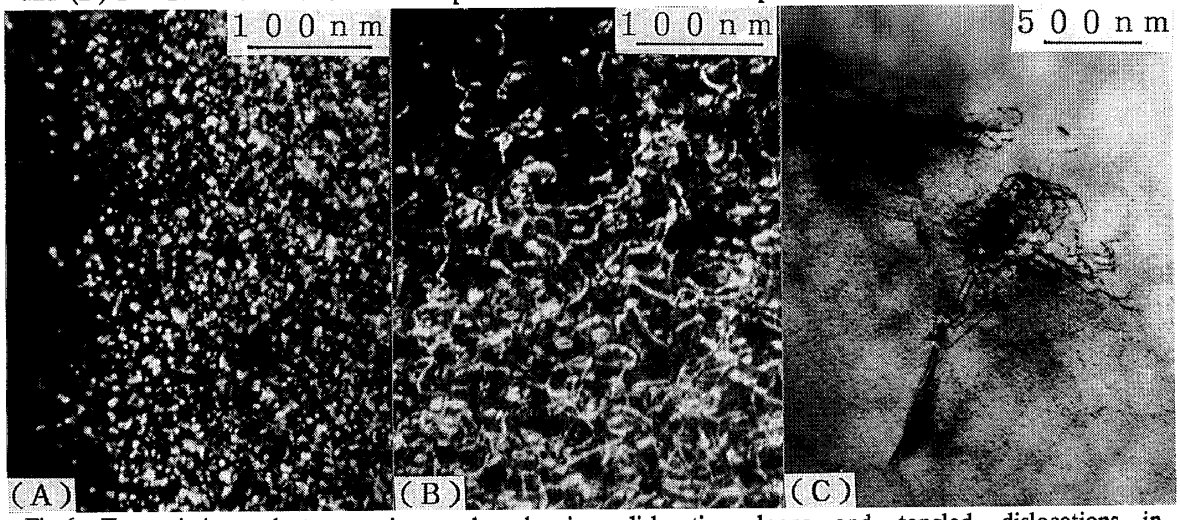

Fig.6 Transmission electron micrographs showing dislocation loops and tangled dislocations in $TiC_{0.85}$ irradiated with fission neutrons of (A) 1×10^{24} n/m^2 at 673 K, (B) 9×10^{25} n/m^2 at 773 K and (C) 1×10^{25} n/m^2 at 873 K in Joyo. The specimens for (A), (B) and (C) were electro-polished, crushed into power and ion-thinned after the irradiation, respectively.

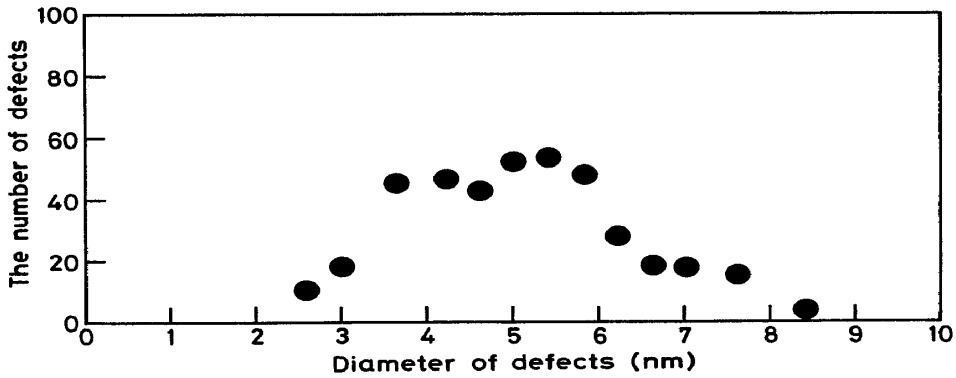

Fig.7 Size distribution of dislocation loops in $TiC_{0.85}$ irradiated with fission neutrons of 1×10^{24} n/m^2 at 673 K in Joyo. The micrograph (A) in fig.6 was used for getting the size distribution and the loop density of 1.9×10^{22} /m^3.

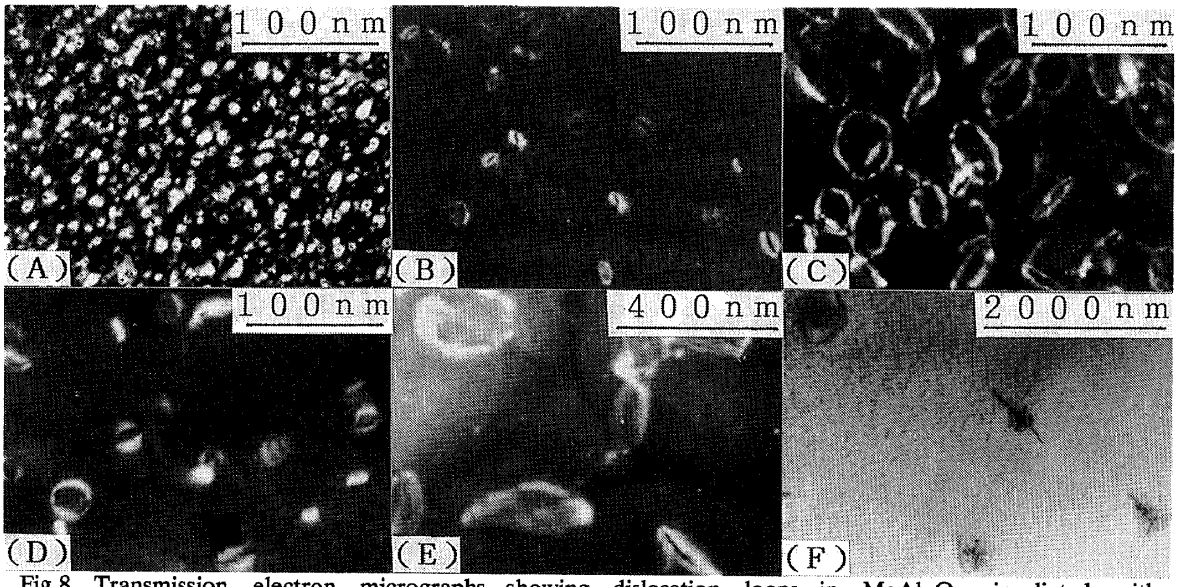

Fig.8 Transmission electron micrographs showing dislocation loops in $MgAl_2O_4$ irradiated with fission neutrons in Joyo. Irradiation conditions are (A) 1×10^{24} n/m^2 at 673 K, (B) 1×10^{25} n/m^2 at 673 K, (C) 9×10^{25} n/m^2 at 673 K, (D) 1×10^{25} n/m^2 at 773 K, (E) 9×10^{25} n/m^2 at 773 K and (F) 1×10^{25} n/m^2 at 873 K. All specimens were crushed into powder after the irradiation.

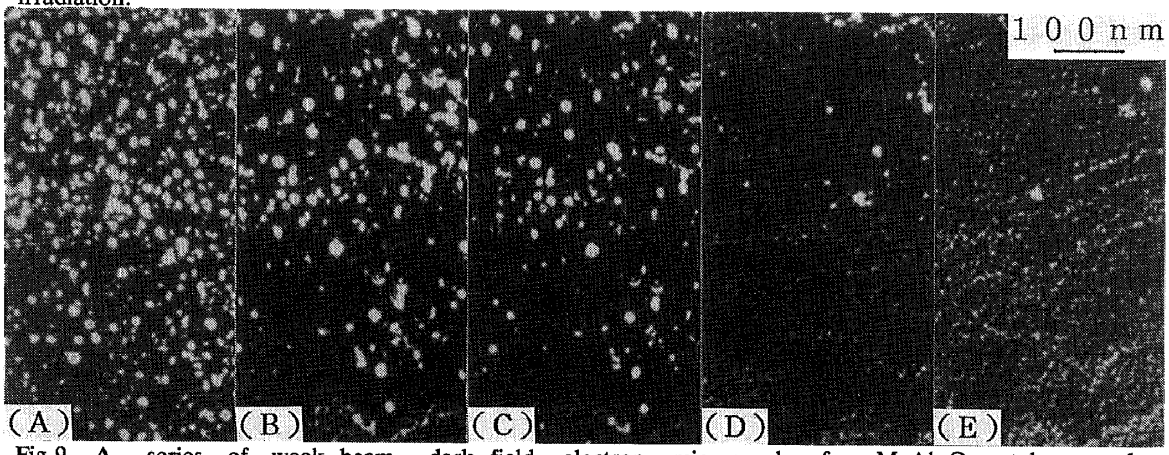

Fig.9 A series of weak-beam dark-field electron micrographs for $MgAl_2O_4$ taken under illumination at 300 K with 200 keV electron flux of 1×10^{23} e/m^{2}s for (A) 360, (B) 540, (C) 840, (D) 1740 and (E) 2160 s. The specimen was ion-thinned and then irradiated with fission neutron fluence of 1×10^{24} n/m^2 at 673 K before the electron illumination.

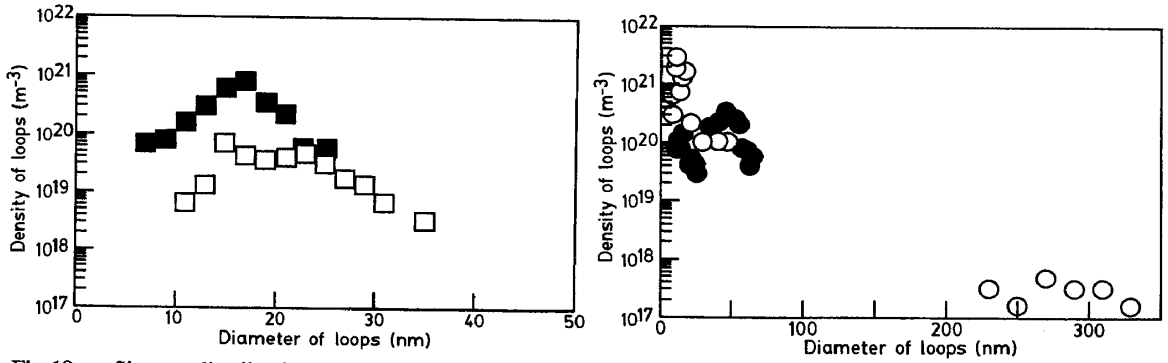

Fig.10 Size distribution of interstitial loops in $MgAl_2O_4$, corresponding to fig.8. Irradiation conditions are as follows ; (■) 1×10^{25} n/m^2 at 673 K, (□) 1×10^{25} n/m^2 at 773 K, (●) 9×10^{25} n/m^2 at 673 K and (○) 9×10^{25} n/m^2 at 773 K. The loop density is 3×10^{20}, 2×10^{19}, 1×10^{20} and 3×10^{17} /m^3 in the order of the preceding conditions.